

SCHOOL OF MATERIALS AND MINERAL RESOURCES ENGINEERING

UNIVERSITI SAINS MALAYSIA

**SYNTHESIS OF ZINC SELENIDE QUANTUM DOTS BY SUCCESSIVE IONIC
LAYER ADSORPTION AND REACTION (SILAR) METHOD FOR QUANTUM DOT
SENSITIZED SOLAR CELLS (QDSSC)**

By

CHANG WAN LING

SUPERVISOR : DR. KHATIJAH AISHA BT. YAACOB

Dissertation submitted in fulfilment

of the requirement for the degree of Bachelor of Engineering with Honours

(Materials Engineering)

Universiti Sains Malaysia

JUNE 2018

DECLARATION

I hereby declare that I have conducted, completed the research work and written the dissertation entitled “**Synthesis of Zinc Selenide Quantum Dots by Successive Ionic Layer Adsorption and Reaction (SILAR) Method for Quantum Dot Sensitized Solar Cells (QDSSCs)**”. I also declare that it has not been previously submitted for the award of any degree or diploma or other similar title of this for any other examining body or University.

Name of Student: Chang Wan Ling

Signature:

Date: 25th June 2018

Witnessed by

Supervisor: Dr. Khatijah Aisha bt. Yaacob

Signature:

Date: 25th June 2018

ACKNOWLEDGEMENTS

After this project period, I would like to express my greatest gratitude to my supervisor Dr. Khatijah Aisha bt. Yaacob who had provided guidance and advice to me in terms of technical and theory as this project was being carried out. Her contribution would not be forgotten.

Besides, I greatly thanks to the dean of School of Materials and Minerals Resources, Engineering Campus of Universiti Sains Malaysia, Prof. Dr. Zuhailawati Hussain for providing such a safe and equipped environment for me to complete my project.

I would like to thank all the academic, administrative, and technical staffs for their endless supports and assistance. Specially appreciation was given to Mr Azam, Mr Azrul, Madam Haslina, Mr Syafiq and Mr Kemuridan for their valuable technical supports and assistances. They are greatly helpful for providing all the apparatus needed and willing to help me handling machines during my lab works. Last but not least, I would like to thank my family members and friends for their endless encouragement and supports during my project period.

TABLE OF CONTENTS

Contents	Page
DECLARATION	II
ACKNOWLEDGEMENTS	III
TABLE OF CONTENTS LIST OF TABLES	IV
LIST OF TABLES	IX
LIST OF FIGURES	XI
LIST OF ABBREVIATIONS	XVII
LIST OF SYMBOLS	XIX
ABSTRAK	XXI
ABSTRACT	XXIII
CHAPTER 1 INTRODUCTION	1
1.1 Research Background	1
1.2 Problem Statement	3
1.3 Research Objectives	4
1.4 Research Scope	5
1.5 Thesis Outline	6
CHAPTER 2 LITERATURE REVIEW	7

2.1	Introduction	7
2.2	Nanomaterials	7
2.3	Solar Cells	8
2.4	Dye Sensitized Solar Cells (DSSCs)	9
2.5	Quantum Dots Sensitized Solar Cells (QDSSCs)	11
2.6	Differences between DSSCs and QDSSCs	12
2.7	Quantum Dots (QDs)	13
2.8	Quantum Confinement	15
2.9	ZnSe QDs	17
2.10	Passivating Layer	18
2.11	Surface treatment	19
2.11.1	Fluoride Treatment	19
2.11.2	Chloride Treatment	20
2.12	Advantages of QDs as Sensitizers	20
2.13	Fabrication of QDs	20
2.13.1	Successive Ionic Layer Adsorption and Reaction (SILAR)	21
2.13.2	Chemical Bath Deposition (CBD)	23
2.14	Applications	24
CHAPTER 3 MATERIALS AND METHODOLOGY		25
3.1	Introduction	25
3.2	Chemicals and Materials	26
3.2.1	Fluorine-doped Tin Oxide (FTO) Glass Substrate	26

3.2.2	Dyesol (R) 18NR-T Titania (TiO ₂) Paste	27
3.2.3	Chemicals	27
3.3	Cleaning of FTO Glass Substrates	29
3.4	Preparation of TiO ₂ Electrode	29
3.5	Fluoride Treatment on TiO ₂ Mesoporous Photoanode	31
3.6	Preparation of ZnSe Sensitizer for TiO ₂ Mesoporous Photoanode	31
3.7	Preparation of Polysulfide Electrolyte Solution	36
3.8	Preparation of Cu ₂ S Counter Electrode	37
3.9	QDSSCs Assembly	38
3.10	Characterization	39
3.10.1	X-Ray Diffraction (XRD)	39
3.10.2	Field Emission Scanning Electron Microscope (FESEM) and Energy Dispersive X-ray Spectroscopy (EDX)	42
3.10.3	High Resolution Transmission Electron Microscope (HRTEM)	42
3.10.4	Atomic Force Microscope (AFM)	43
3.10.5	UV-Visible Spectroscopy (UV-vis)	44
3.10.6	Conductivity Test	45
3.10.7	Current density-Voltage (<i>J-V</i>) measurement	46
CHAPTER 4 RESULTS AND DISCUSSION		49
4.1	Introduction	49
4.2	Conductivity Test	49
4.3	FTO Glass and TiO ₂ Electrode	50

4.3.1	Structural Analysis	51
4.3.2	Surface Morphology	53
4.3.3	Elemental Analysis	56
4.3.4	Surface Roughness	57
4.3.5	Band Gap	60
4.4	FTO/ZnSe and FTO/TiO ₂ /ZnSe (with and without fluoride treatment)....	62
4.4.1	Structural Analysis	63
4.4.2	Band Gap	64
4.4.3	Characterization of QDSSCs	67
4.5	FTO/TiO ₂ /ZnSe/ZnS	71
4.5.1	Structural Analysis	73
4.5.2	Characterization of QDSSCs	74
4.6	FTO/TiO ₂ /ZnSe with different number of SILAR cycles for ZnSe QDs sensitization	77
4.6.1	Surface Morphology	78
4.6.2	Elemental Analysis	81
4.6.3	Band Gap	85
4.6.4	Characterization of QDSSCs	87
4.7	FTO/TiO ₂ /ZnSe Synthesized with Different Molar Concentration of Zinc Acetate Dihydrate Solution	89
4.7.1	Band Gap	90
4.7.2	Characterization of QDSSCs	92
4.8	High Resolution Transmission Electron Microscope (HRTEM)	95

CHAPTER 5 CONCLUSION AND RECOMMENDATIONS	97
5.1 Conclusion	97
5.2 Recommendations	98
REFERENCES	100

LIST OF TABLES

Contents	Page
Table 3.1: Description of FTO glass	26
Table 3.2: Description of Dyesol (R) 18NR-T titania (TiO ₂) paste	27
Table 3.3: Descriptions of chemical formula, supplier and function of each chemical used	28
Table 3.4: Weight of chemicals needed to produce cationic and anionic precursors of ZnSe QDs	32
Table 3.5: Weight of zinc acetate dihydrate powder for different molar concentration of Zn(CH ₃ COO) ₂ ·2H ₂ O solution in 30 ml	35
Table 3.6: Weight of chemicals needed to produce cationic and anionic precursors of ZnS QDs	36
Table 3.7: Weight of chemicals needed to produce polysulfide electrolyte solution	37
Table 4.1: Interplanar spacing and crystallite size of FTO glass and TiO ₂ electrode	53
Table 4.2: Band gap and absorption edge for FTO/ZnSe, FTO/TiO ₂ /ZnSe with and without fluoride treatment on TiO ₂ mesoporous film	66
Table 4.3: Open circuit voltage, V_{OC} ; short circuit current, J_{SC} ; fill factor, FF and efficiency, η of FTO/ZnSe, FTO/TiO ₂ /ZnSe with and without fluoride treatment	70

Table 4.4: Interplanar spacing and crystallite size of FTO/TiO ₂ /ZnSe/ZnS (with blocking layer) and FTO/TiO ₂ /ZnSe (without blocking layer)	74
Table 4.5: Open circuit voltage, V_{OC} ; short circuit current, J_{SC} ; fill factor, FF and efficiency, η of FTO/TiO ₂ /ZnSe/ZnS and FTO/TiO ₂ /ZnSe two weeks after the sample preparation	77
Table 4.6: Average particle size of ZnSe QDs with different number of SILAR cycles	80
Table 4.7: Weight percentage of each element in FTO/TiO ₂ /ZnSe with different number of SILAR cycles	84
Table 4.8: Band gap and absorption edge for FTO/TiO ₂ /ZnSe with different number of SILAR cycles	87
Table 4.9: Open circuit voltage, V_{OC} ; short circuit current, J_{SC} ; fill factor, FF and efficiency, η of FTO/TiO ₂ /ZnSe with different number of SILAR cycles	88
Table 4.10: Band gap and absorption edge for FTO/TiO ₂ /ZnSe synthesized with different molar concentration of zinc acetate dihydrate solution	92
Table 4.11: Open circuit voltage, V_{OC} ; short circuit current, J_{SC} ; fill factor, FF and efficiency, η of FTO/TiO ₂ /ZnSe with different molar concentration of zinc acetate dihydrate solution	94

LIST OF FIGURES

Contents	Page
Figure 1.1: The general scheme of a typical QDSC device (Meng et al., 2015)	1
Figure 2.1: Illustration of the interfacial charge-transfer processes occurring at the nanostructured TiO ₂ /dye/electrolyte interface of DSSC (Palomares et al., 2002)	10
Figure 2.2: Schematic depiction of multiple exciton generation (MEG) and extraction (Zhang et al., 2015)	15
Figure 2.3: Quantum confinement in QDs (Rabouw and de Mello Donega, 2016)	17
Figure 2.4: Schematic representation of SILAR deposition (Lee <i>et al.</i> , 2010)	21
Figure 3.1: Flow chart of sample preparation and characterization steps involved in QDSSCs	25
Figure 3.2: Doctor blade technique used to deposit TiO ₂ paste on FTO glass substrate	29
Figure 3.3: Sintering profile of TiO ₂ electrode at 450 °C	30
Figure 3.4: Deposition of yellow TiO ₂ paste on FTO glass substrate before sintering, (b) transparent TiO ₂ mesoporous film formed after sintering	31
Figure 3.5: Schematic diagram of refluxing of sodium selenosulphate, Na ₂ SeSO ₄ solution	32

Figure 3.6: Brass plate before immersion in heated HCl, (a) after immersion in heated HCl, changed to brownish colour, (c) after treated with polysulfide solution	38
Figure 3.7: Assembly of QDSSCs	38
Figure 3.8: Bragg diffraction by crystal planes	41
Figure 3.9: AFM is working with an optical lever	44
Figure 3.10: $J-V$ measurement set up	47
Figure 3.11: Current–voltage (I-V) curves of a photovoltaic solar cell under dark and	47
Figure 4.1: The conductivity value of polysulfide electrolyte	50
Figure 4.2: FTO glass with transparent TiO ₂ mesoporous film indicated in red box	50
Figure 4.3: XRD diffraction patterns of (a) FTO glass and (b) TiO ₂ electrode	52
Figure 4.4: FESEM image of FTO glass at magnification of 30 kX	54
Figure 4.5: FESEM surface morphology of TiO ₂ electrode at a magnification of 50 kX	55
Figure 4.6: FESEM cross-sectional area image of TiO ₂ electrode at magnification	56
Figure 4.7: EDX analysis of FTO glass	57
Figure 4.8: EDX analysis of TiO ₂ electrode	57

Figure 4.9: AFM images of (a) 3-dimensional, and (b) 2-dimensional topography, of FTO glass substrate over scanning area of 10 μm x 10 μm	58
Figure 4.10: AFM images of (a) 3-dimensional, and (b) 2-dimensional topography, of TiO ₂ electrode over scanning area of 10 μm x 10 μm	59
Figure 4.11: AFM images of (a) 3-dimensional, and (b) 2-dimensional topography, of FTO/TiO ₂ /ZnSe over scanning area of 10 μm x 10 μm	60
Figure 4.12: RMS surface roughness for FTO glass, TiO ₂ electrode, and FTO/TiO ₂ /ZnSe	60
Figure 4.13: UV-visible absorption spectrum of TiO ₂ electrode	61
Figure 4.14: Plot of $(ah\nu)^2$ versus $h\nu$ for TiO ₂ electrode	62
Figure 4.15: (a) and (b) are the TiO ₂ electrode with and without fluoride treatment respectively, ZnSe QDs sensitized on (c) TiO ₂ mesoporous film with fluoride treatment, (d) TiO ₂ mesoporous film without fluoride treatment, and (e) on bare FTO glass substrate	63
Figure 4.16: XRD diffraction patterns of (a) FTO/ZnSe, (b) FTO/TiO ₂ /ZnSe (with fluoride treatment), and (c) FTO/TiO ₂ /ZnSe (without fluoride treatment)	64
Figure 4.17: UV-visible absorption spectra of FTO/ZnSe, FTO/TiO ₂ /ZnSe with and without fluoride treatment on TiO ₂ mesoporous film	65
Figure 4.18: Plot of $(ah\nu)^{0.5}$ versus $h\nu$ for FTO/ZnSe, FTO/TiO ₂ /ZnSe with and without fluoride treatment on TiO ₂ mesoporous film	66

Figure 4.19: J - V curve for all samples under dark condition	67
Figure 4.20: J - V curve for FTO/ZnSe, FTO/TiO ₂ /ZnSe with and without fluoride treatment on TiO ₂ mesoporous film	68
Figure 4.21: Energy band diagram showing the charge transfer processes in (a) QDSSC and (b) QD _{FTO} (Shalom et al., 2011)	69
Figure 4.22: Efficiency for FTO/ZnSe, FTO/TiO ₂ /ZnSe with and without fluoride treatment	71
Figure 4.23: TiO ₂ mesoporous film (a) after five SILAR cycles of ZnSe QDs sensitization, and (b) after five SILAR cycles of ZnSe QDs sensitization and two SILAR cycles of ZnS QDs deposition as blocking layer	72
Figure 4.24: (a) and (b) are TiO ₂ electrodes with and without ZnS blocking layer respectively, while (c) and (d) are TiO ₂ electrodes with and without ZnS blocking layer after two weeks	72
Figure 4.25: XRD diffraction patterns of (a) FTO/TiO ₂ /ZnSe/ZnS and (b) FTO/TiO ₂ /ZnSe (without blocking layer)	73
Figure 4.26: J - V curve for FTO/TiO ₂ /ZnSe/ZnS and FTO/TiO ₂ /ZnSe two weeks after sample preparation	75
Figure 4.27: Schematic diagram of the TiO ₂ /ZnSe/ZnS and the band gap edge alignment of TiO ₂ , ZnSe and ZnS (Niu et al., 2010)	76

Figure 4.28: Efficiency for FTO/TiO ₂ /ZnSe/ZnS and FTO/TiO ₂ /ZnSe two weeks after sample preparation	77
Figure 4.29: TiO ₂ electrodes with different number of SILAR cycles of ZnSe QDs sensitization	78
Figure 4.30: FESEM image of FTO/TiO ₂ /ZnSe with (a) 5 SILAR cycles, (b) 10 SILAR cycles, (c) 15 SILAR cycles, (d) 20 SILAR cycles, and (e) 25 SILAR cycles, at 150 kX	80
Figure 4.31: Average particle size of ZnSe QDs with different number of SILAR cycles	81
Figure 4.32: EDX analysis of FTO/TiO ₂ /ZnSe with 5 SILAR cycles	82
Figure 4.33: EDX analysis of FTO/TiO ₂ /ZnSe with 10 SILAR cycles	82
Figure 4.34: EDX analysis of FTO/TiO ₂ /ZnSe with 15 SILAR cycles	83
Figure 4.35: EDX analysis of FTO/TiO ₂ /ZnSe with 20 SILAR cycles	83
Figure 4.36: EDX analysis of FTO/TiO ₂ /ZnSe with 25 SILAR cycles	84
Figure 4.37: Weight percentage of each element in FTO/TiO ₂ /ZnSe with different number of SILAR cycles	85
Figure 4.38: UV-visible absorption spectra of FTO/TiO ₂ /ZnSe with different number of SILAR cycles	86
Figure 4.39: Plot of $(ah\nu)^{0.5}$ versus $h\nu$ for FTO/TiO ₂ /ZnSe with different number of SILAR cycles	86

Figure 4.40: J - V curve FTO/TiO ₂ /ZnSe with different number of SILAR cycles	87
Figure 4.41: Efficiency for FTO/TiO ₂ /ZnSe with different number of SILAR cycles	89
Figure 4.42: TiO ₂ electrodes sensitized with different molar concentration of zinc acetate dihydrate solution	90
Figure 4.43: UV-visible absorption spectra of FTO/TiO ₂ /ZnSe synthesized with different molar concentration of zinc acetate dihydrate solution	91
Figure 4.44: Plot of $(ah\nu)^{0.5}$ versus $h\nu$ for FTO/TiO ₂ /ZnSe synthesized with different molar concentration of zinc acetate dihydrate solution	92
Figure 4.45: J - V curve of FTO/TiO ₂ /ZnSe with different molar concentration of zinc acetate dihydrate solution	93
Figure 4.46: Efficiency, η of FTO/TiO ₂ /ZnSe with different molar concentration of zinc acetate dihydrate solution	95
Figure 4.47: HRTEM image of TiO ₂ nanoparticles with ZnSe quantum dots deposited with 20 SILAR cycles when 0.1 M zinc acetate dihydrate solution was used, at scale of (a) 100 nm, (b) 50 nm, (c) 20 nm, and (d) 10 nm	96

LIST OF ABBREVIATIONS

2D	Two-Dimensional
3D	Three-Dimensional
AFM	Atomic Force Microscopy
CB	Conduction Band
CBD	Chemical Bath Deposition
CE	Counter Electrode
DSSCs	Dye Sensitized Solar Cells
EDX	Energy Dispersive X-Ray
EDX	Energy Dispersive X-Ray
FESEM	Field Emission Scanning Electron Microscopy
FF	Fill Factor
FTO	Fluorine Doped Tin Oxide
HOMO	Highest Occupied Molecular Orbital
HRTEM	High Resolution Transmission Electron Microscopy
J-V	Current density-Voltage
LUMO	Lowest Unoccupied Molecular Orbital
MEG	Multiple Exciton Generation
nm	Nanometer
QDs	Quantum Dots
QDSSCs	Quantum Dot Sensitized Solar Cells
RMS	Root Mean Square

SILAR	Successive Ionic Layer Adsorption and Reaction
UV	Ultraviolet
V	Voltage
VB	Valence Band
WE	Working Electrode
XRD	X-ray Diffraction
μm	Micron meter

LIST OF SYMBOLS

%	Percentage
<	Less than
°C	Degree Celsius
At%	Atomic Percent
E_g	Band Gap Energy
eV	Electron Volt
g	Gram
h	Planck Constant
\hbar^2	Reduced Planck Constant
J_{mp}	Current Density at Maximum Point
J_{sc}	Short-Circuit Current
M	Molar Concentration
ml	Millilitre
P_{in}	Incident Solar Power Density
V	Volume
V_{mp}	Voltage at Maximum Point
V_{oc}	Open Circuit Voltage
Wt%	Weight Percent
η	Efficiency
a	Exciton Bohr Radius
v	Speed of Light

m_h	Effective Mass of a Hole
m_e	Effective Mass of an Electron
r	Radius of the quantum dots
ε	Dielectric Constant
λ	Wavelength

**SINTESIS TITIK KUANTUM ZINK SELENAID DENGAN KAEDAH PENJERAPAN
DAN TINDAKBALAS LAPISAN BERTURUT-ION (SILAR) UNTUK SEL SURIA
SENSITIF TITIK KUANTUM (QDSSC)**

ABSTRAK

Sel-sel suria sensitif titik kuantum (QDSSCs) telah menjadi perhatian secara intensif sejak beberapa dekad yang lalu. Titik kuantum (QD) zink selenaid (ZnSe) merupakan satu bahan alternatif untuk menggantikan QD berasaskan kadmium yang bertoksik. Dalam kajian ini, QD ZnSe telah dimendapkan atas elektrod TiO₂ sebagai fotoanod TiO₂ dengan kaedah penjerapan dan tindakbalas lapisan berturut-ion (SILAR) untuk QDSSCs. Elektrod TiO₂ dibentuk dengan pemendapan lapisan TiO₂ berliang meso di atas kaca oksida timah berdopkan fluorin (FTO) setelah pemanasan pada suhu 370 °C untuk 10 minit, suhu ditingkatkan ke 450 °C dan dikekalkan untuk 30 minit. Sel-sel suria disediakan dengan mengapitkan fotoanod TiO₂ dan fotokatod Cu₂S dengan larutan polisulfid di tengah. Kesan rawatan fluorida atas lapisan TiO₂ berliang meso sebelum pemendapan titik kuantum ZnSe, bilangan kitaran SILAR (5, 10, 15, 20 dan 25), kepekatan molar larutan zink asetat dihidrat (0.03 M, 0.05 M, 0.1 M, 0.3 M and 0.5 M), dan kesan salutan lapisan penyekat ZnS selepas lapisan ZnSe telah dipelajari. Sampel-sampel disediakan dan dicirikan dengan pembelauan sinar-X (XRD), mikroskop pengimbasan elektron medan pelepasan (FESEM), spektroskopi sinar-X penyebaran tenaga (EDX), mikroskop penghantaran elektron resolusi tinggi (HRTEM), mikroskop daya atomik (AFM), spektroskopi UV-vis (UV-vis), dan pengukuran ketumpatan arus-voltan ($J-V$). Lapisan penyekat ZnS didapati tidak menyumbang dalam memperbaiki kecekapan QDSSCs kerana jurang jalur yang lebar iaitu 3.10 eV. Secara

amnya, apabila bilangan kitaran SILAR dan kepekatan molar larutan meningkat, kecekapan akan meningkat disebabkan semakin banyak nukleus ZnSe bersaiz lebih besar akan dibentuk dalam lapisan TiO₂ berliang meso. Walau bagaimanapun, penyumbatan liang atas lapisan TiO₂ berliang meso bermungkinan berlaku disebabkan QD berlebihan. Sampel dengan 20 kitaran SILAR menunjukkan kecekapan tertinggi iaitu 0.6988 %, sementara sampel yang dimendapan dengan 0.1 M larutan zink asetat dihidrat menunjukkan kecekapan iaitu 0.5956 %. Sampel dengan rawatan fluorida atas lapisan TiO₂ berliang meso juga menunjukkan kecekapan yang lebih tinggi iaitu 0.4485 % daripada yang tiada rawatan fluorida iaitu 0.0679 %. Dalam kajian ini, hasil-hasilan boleh disimpulkan untuk mencadangkan supaya menjalankan rawatan fluorida atas lapisan TiO₂ berliang meso sebelum pemendapan 20 kitaran SILAR ZnSe QDs dengan 0.1 M larutan zink asetat dihidrat.

**SYNTHESIS OF ZINC SELENIDE QUANTUM DOTS BY SUCCESSIVE IONIC LAYER
ADSORPTION AND REACTION (SILAR) METHOD FOR QUANTUM DOT
SENSITIZED SOLAR CELL (QDSSC)**

ABSTRACT

Quantum dot sensitized solar cells (QDSSCs) have been intensively concerned in the past decades. Zinc selenide (ZnSe) is an alternative material to replace toxic cadmium-based quantum dots (QDs). In this research, ZnSe QDs were deposited on TiO₂ electrode as TiO₂ photoanode using successive ionic layer adsorption and reaction (SILAR) method for QDSSCs. TiO₂ electrode was formed with the deposition of TiO₂ mesoporous film on fluorine doped tin oxide (FTO) glass after the sintering in furnace at 370 °C for 10 minutes, the temperature was increased to 450 °C and held for 30 minutes. Solar cells were prepared by sandwiching the TiO₂ photoanode and Cu₂S counter electrode with polysulfide electrolyte in the between. Effect of fluoride treatment on TiO₂ mesoporous film prior to deposition of ZnSe QDs, number of SILAR cycles (5, 10, 15, 20 and 25), molar concentration of zinc acetate dihydrate solution (0.03 M, 0.05 M, 0.1 M, 0.3 M and 0.5 M), and the effect of ZnS blocking layer coating after ZnSe layer was studied. The samples were prepared and characterized with X-ray diffraction (XRD), field emission scanning electron microscope (FESEM), energy dispersive X-ray spectroscopy (EDX), high resolution transmission electron microscope (HRTEM), atomic force microscope (AFM), UV-visible (UV-vis) spectroscopy, and current density-voltage (*J-V*) measurement. ZnS blocking layer was found that did not contribute in improving the efficiency of QDSSCs due to its wide band gap of 3.10 eV. Generally, as number of SILAR cycles and molar concentration of

precursor solution increased, the efficiency increased due to more and bigger ZnSe nuclei were formed in the TiO₂ mesoporous film. However, pore-blocking on the TiO₂ mesoporous structure may occur due to overloading of QDs. Sample with 20 SILAR cycles shows the highest efficiency of 0.6988 % while deposition using 0.1 M zinc acetate dihydrate solution shows efficiency of 0.5956 %. The sample with fluoride treatment on TiO₂ mesoporous film also shows the higher efficiency of 0.4485 % than without fluoride treatment of 0.0679 %. In this research, the results can be concluded to suggest to carry out fluoride treatment on TiO₂ mesoporous film prior deposition of 20 SILAR cycles of ZnSe QDs with 0.1 M of zinc acetate dihydrate solution.

CHAPTER 1

INTRODUCTION

1.1 Research Background

Due to the arising concern of global warming and the demand for renewable energy becomes more critical every day, low cost and high power conversion efficiency photovoltaic devices are needed. Dye sensitized solar cells (DSSCs) have attracted attention over the past two decades regardless in academic study or industrial field because DSSCs are the potential photovoltaic devices compared to the conventional silicon. DSSCs employ a monolayer of inorganic molecular dye as light harvesting medium, attached to mesoscopic metal oxide film (typically anatase titanium dioxide, TiO_2), achieving power conversion efficiency of 28 %, while the silicon solar cells achieve efficiency of 15.6 % (Rasheduzzaman et al., 2016). Apart from inorganic molecular dyes, quantum dots (QDs) deposited on TiO_2 film are receiving considerable attention to take over dyes because of their ability to tune the optical properties and band gap (Salant et al., 2010; Singh et al., 2012). Figure 1.1 shows the general scheme of a typical QDSC device.

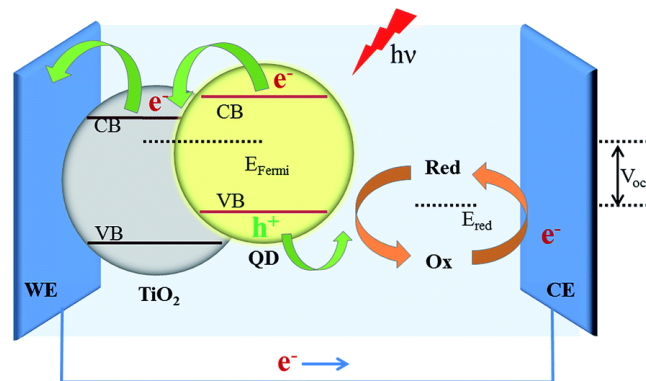


Figure 1.1: The general scheme of a typical QDSC device (Meng et al., 2015)

From the last few decades, researchers were focused on DSSCs, but shifted their direction and goals to QDSSCs due to the wastage of photon energy more than the band energy between lowest unoccupied molecular orbital (LUMO) and highest occupied molecular orbital (HOMO). One photon can only give rise to one exciton, the remaining energy in the photon is wasted as heat. The advantage of QDSSCs over DSSCs is the multiple exciton generation (MEG) effect, which one photon can give rise to multiple exciton to improve the efficiency of solar cells (Singh et al., 2012). Earlier report has been done to study on thermodynamic of the theoretical enhancement of the conversion efficiency in solar cells that are based on MEG in QDs (Nozik, 2008).

Examples of QDs are II-VI semiconducting materials: CdTe, CdSe, CdS, ZnSe and ZnS. These are wide band gap, high absorption coefficients, high binding energy, high chemical stability, and environment-friendly semiconductors (Hassanien and A Akl, 2015).

Cadmium-based QDs has been widely used in various applications, but due to the cytotoxicity of heavy metal Cd^{2+} ions, may result in potential *in vitro* toxicity that hampers their practical applications. Hence, researchers started to look for alternative materials to replace Cd-based QDs (Chen et al., 2012).

Zinc-based QDs like ZnSe is an alternative material to form QDs due to its wide band gap. ZnSe can effectively cover TiO_2 , resulting in strong inhibition of the electron leakage from either TiO_2 or QDs to the electrolyte, thereby significantly improving the photovoltaic performance of QDSSCs (Gopi et al., 2015). Moreover, ZnSe is environmental friendly, compared to Cd-based QDs. In this study, ZnSe nanocrystals were grown on TiO_2 mesoporous film as major light absorbing materials in QDSSCs.

In this research, successive ionic layer adsorption and reaction (SILAR) was used to deposit the ZnSe QDs on TiO₂. SILAR is considered as an effective way to prepare QDs sensitizers on mesoporous metal oxides. Shorter fabrication time, higher surface coverage and close stoichiometry formation are the advantages of SILAR method compared to chemical bath deposition (CBD) (Senthamilselvi et al., 2012).

1.2 Problem Statement

Cadmium-based quantum dots (QDs) are increasingly applied in existing and emerging technologies, especially in biological applications due to their exceptional photophysical and functionalization properties. However, they are very toxic compounds due to the high reactive and toxic cadmium core (Silva et al., 2016). Therefore, it is important to look for alternative materials which can replace Cd-based QDs without neglecting their high potential utilization in applications. ZnSe is usually used as passivating layer in core/shell structure QDs due to its wide band gap. In this study, ZnSe QDs were used as major light harvesting materials instead of Cd-based QDs.

In this research, TiO₂ mesoporous film was deposited on the fluorine doped tin oxide (FTO) glass as TiO₂ electrode. However, TiO₂ has a relatively small exciton radius with less than ~1 nm which does not show the quantum confinement effect. This is because in order to show strong quantum confinement effect, the atomic radius of the particle needs to be much smaller than its Bohr radius, this is hard to achieve by TiO₂ with small exciton radius. Therefore, ZnSe QDs were deposited on TiO₂ mesoporous film as sensitizer with SILAR

method. The bulk band gap of ZnSe (2.70 eV) can be manipulated by controlling its particle size to reach the quantum confinement effect.

In the first report of photochemical cells (Lee et al., 2009), dye was not efficient as sensitizers in metal oxide solar cells, because they are lack of hole carriers, hence in QDs were used instead of conventional dye materials as sensitizer.

To grow well-defined ZnSe crystals, the toxic precursor, H₂Se is required (Borchert et al., 2003). One of disadvantages of II-VI chalcogenide semiconductors is the instability of anions (i.e. Se, Te) in aqueous phase, hence the reduction in water usually used high reductive agent, NaBH₄ which was in high pH. In this study, Na₂S will replace the NaBH₄ which has high pH value, to reduce the Se²⁻ ions.

1.3 Research Objectives

Objectives of this research are as followed:

- (a) To study the effect of fluoride treatment on TiO₂ mesoporous film prior ZnSe quantum dots sensitization, to the performance of quantum dot sensitized solar cells.
- (b) To investigate the effect of SILAR cycles to the properties and performance of quantum dot sensitized solar cells.
- (c) To investigate the effect of molar concentration of the zinc acetate dihydrate solution to the properties and performance of quantum dot sensitized solar cells.
- (d) To investigate the effect of ZnS blocking layer coating on the performance of quantum dot sensitized solar cells.

1.4 Research Scope

Firstly, fluorine doped tin oxide (FTO) glass was characterized with X-ray diffraction (XRD), field emission scanning electron microscope (FESEM) and energy dispersive X-ray spectroscopy (EDX). Then, TiO₂ electrode was characterized with the same methods as FTO glass, with addition of UV-visible spectrometer (UV-vis).

Two samples which were FTO/TiO₂/ZnSe and FTO/TiO₂/ZnSe/ZnS were studied with XRD and UV-vis spectrometer. Then, one sample FTO/ZnSe and two samples FTO/TiO₂/ZnSe (with and without fluoride treatment on the TiO₂ mesoporous film prior to deposition of ZnSe QDs) were prepared and characterized with XRD, FESEM, EDX, UV-vis spectrometer and AFM.

Five samples of FTO/TiO₂/ZnSe with different number of SILAR cycles of ZnSe QDs deposition which were 5, 10, 15, 20 and 25, were prepared and characterized with FESEM, EDX and UV-vis spectrometer. Another five samples of FTO/TiO₂/ZnSe which were deposited with different molar concentration of zinc acetate dihydrate solution (0.03 M, 0.05 M, 0.1 M, 0.3 M and 0.5 M) were prepared and characterized with UV-vis spectrometer.

FTO glass, TiO₂ electrode and FTO/TiO₂/ZnSe with fluoride treatment on TiO₂ mesoporous film prior to 20 SILAR cycles of ZnSe QDs deposition in 0.1 M zinc acetate dihydrate solution, were examined with atomic force microscope (AFM). The same sample of FTO/TiO₂/ZnSe was also characterized with high resolution transmission electron microscope (HRTEM).

Lastly, all samples were assembled as QDSSCs by sandwiching the TiO₂ photoanode and Cu₂S counter electrode with polysulfide electrolyte solution in between both electrodes. Current density-voltage (*J-V*) measurement were carried out on these samples.

1.5 Thesis Outline

This report consists of five chapters. Chapter 1 includes introduction, objectives and research scope of present work. The introduction elaborates DSSCs, QDSSCs, ZnSe and SILAR method. Chapter 2 provides better understanding of background literature review relevant to present work. Chapter 3 describes raw materials, chemicals used, experimental procedure, characterization and *J-V* measurement. Lastly, Chapter 5 presents conclusion for the whole project and recommendations for future studies.

CHAPTER 2

LITERATURE REVIEW

2.1 Introduction

Solar energy is renewable resource which has high potential to generate various kinds of energy as solar energy is the most abundant energy source on the planet. As well as concerns like global warming and air pollution, people started to implement the massive growth in solar energy industry due to the high demand for energy consumption. It is the alternative source for fossil fuels which were mostly used to generate energy in past decades. Due to nanomaterials has been intensively researched, the study on conventional dye-sensitized solar cells (DSSCs) was enhanced by development of quantum dot-sensitized solar cells (QDSSCs). In this chapter, the history background of nanomaterials, DSSCs, QDSSCs, quantum dots (QDs) and basic principle of QDSSCs, types of QDs, synthesis of QDs and its applications will be discussed.

2.2 Nanomaterials

Nanoscale materials are defined as a set of substances where at least one dimension is less than approximately 100 nanometers. Nanomaterials are receiving intensive attentions because at this scale unique optical, magnetic, electrical, and other properties emerge. These properties have the potential for applications in electronics, medicine, and other fields (A, 2011). Nanomaterials with a few atoms in size, are extremely tiny substances, which can have unique properties to those in usual form. However, these unique properties might imply

to increase of risk and hazards to humans and environment because its tiny size allow them to enter human body easily and spread throughout the body.

The tiny size of substances also makes them have large surface area, hence increase the rate of reaction with other substances which occur on the surface of the materials. This small dimension of nanomaterials causes them to have high potential to form intimate mixtures to enhance the properties of other materials, especially in photovoltaic devices.

2.3 Solar Cells

While solar energy could provide enough power to satisfy the current worldwide demand, the fabrication of photovoltaic systems that are efficient and competitive with fossil fuels remains a serious challenge. To solve this problem, new strategies for solar-to-electric energy conversion are under development. Many of these strategies utilize the following sequence of physical processes: (a) a light-absorbing material generates an electron-hole pair, (b) the electron and hole separate quickly into two different phases, and (c) the carriers are transported in these respective phases to opposing electrodes. During each of these steps, efficiency requires that charge recombination is minimized (Leschkies et al., 2007).

One classic example of such a photovoltaic device is the dye-sensitized solar cell, in which light is absorbed by dye molecules adsorbed at the interface between a network of TiO₂ nanoparticles and a hole conducting liquid electrolyte (Dürr et al., 2004). Another example is the bulk heterojunction solar cell, in which two immiscible transport materials are blended to form a three-dimensional bi-continuous network. In this case, light is absorbed

by either phase, but the photogenerated electrons and holes can quickly dissociate into separate phases because the the interfacial boundary is always nearby. Both organic and inorganic materials have been used to demonstrate this approach. However, despite the successes of dye sensitized and bulk heterojunction solar cells, new combinations of materials and device architectures are still sought to improve further the performance and cost of solar cells (Leschkies et al., 2007).

2.4 Dye Sensitized Solar Cells (DSSCs)

In the last decade, dye-sensitised solar cells (DSSCs) have been developed into one of the most interesting alternatives to current solar cell technology for the conversion of sunlight into electrical energy.

DSSCs consist of a sensitizing dye, transparent conducting substrates (F-doped tin oxide), nanometer sized TiO_2 film, iodide electrolyte, and counter electrode (Pt or carbon). When a dye molecule absorbs light, it excites electrons on the highest occupied molecular orbital to the lowest unoccupied molecular orbital. The excited dye molecule injects an electron into the conducting band of the TiO_2 film. The oxidized dye is restored by electron donation from the reducing ions in the electrolyte, usually an organic solvent containing a redox system. The donated electron is in turn regenerated by the reduction of conjugated ions in the electrolytes. The circuit is completed by electron migration through an external load (Lee et al., 2010b).

Efficiency of the DSSC device depends on the least possible recombination pathways occurring at the TiO_2 /dye/electrolyte interface, allowing efficient charge transport through the TiO_2 film and electrolyte and subsequent charge collection at the device contacts. From Figure 2.1, there are two possible recombination losses to consider. The injected electrons may recombine either with oxidized dye molecules (3) or with the oxidised redox couple (5); the latter reaction is thought to be particularly critical to device function (Palomares et al., 2002).

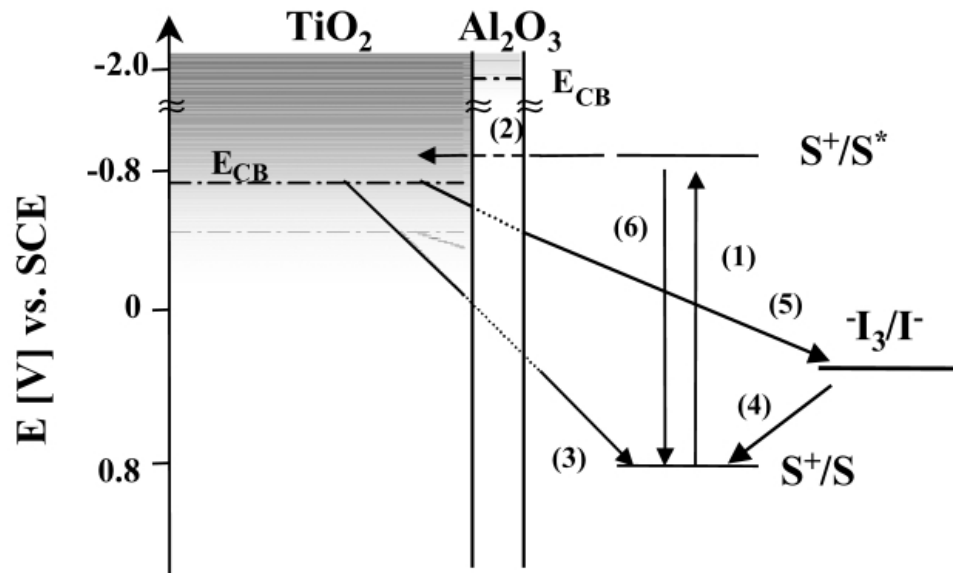


Figure 2.1: Illustration of the interfacial charge-transfer processes occurring at the nanostructured TiO_2 /dye/electrolyte interface of DSSC (Palomares et al., 2002)

The disadvantage of the DSSCs is the high band gap of the core materials, for example, TiO_2 nanoparticles which have 3.20 eV, wavelength <385 nm in ultraviolet (UV) range. In solar UV light spectrum, only 2 -3 % of the sunlight can be utilized, hence dye sensitizers are employed to assist in moving the charge to TiO_2 by absorbing visible light at injecting electrons. The cost of DSSC production is 30% that of traditional silicon solar cells,

and theoretically, the conversion efficiency can be increased to 33% with less environmental damage (Lee et al., 2010b).

2.5 Quantum Dots Sensitized Solar Cells (QDSSCs)

The key development of QDSSC was made by Kamat in 2005, with the pre-synthesized CdSe nanocrystals linked to TiO₂ thin films by organic molecules (Robel et al., 2006). Since then various methods of sensitization have been developed, and they can be summarized into two main categories: assembly of pre-synthesized QDs and direct growth (Luo et al., 2012).

Pre-synthesis provides the feasibility of facile control in the size, size distribution and morphology. However, the charge transfer would be retarded by the surface functional molecules. Also the loading of the sensitizer prepared by this method is usually low.

Direct growth allows both a compact contact of the sensitizer with TiO₂, and the ease of increasing the loading of the sensitizer. A diverse range of methods are reported for the direct coating of the sensitizing materials, such as chemical bath deposition, successive ionic layer adsorption and reaction (SILAR), electrochemical deposition, chemical vapour deposition and electrophoretic deposition.

Although much effort has been devoted to the development of QDSSCs, their photovoltaic efficiency is still relatively low. One major challenge in this field is how to

assemble QDs into the mesoporous TiO₂ matrix to obtain a well-covered monolayer (Li et al., 2011).

2.6 Differences between DSSCs and QDSSCs

In a DSSC, the photosensitizing dye, adsorbed on the nanocrystalline TiO₂ film, plays an important role in determining the light absorption and subsequent electron-transfer process, and has been regarded as one of the key factors to govern the light-to-electricity conversion efficiency (η) of the cell (Yeh et al., 2011).

Narrow band gap semiconductor quantum dots (QDs), such as CdS, CdSe, PbS, PbSe, InP, InAs, and ZnSe have been introduced as photo sensitizers for solar cells. The distinctive characteristics of QDs over the conventional dyes are their strong photo-response in the visible region and their quantum confinement effects (Yu et al., 2006). Moreover, QDs possess tunable optical properties and band gaps depending on the particle size (quantum size effect). Higher conversion efficiencies for QDSSCs are expected to be obtained owing to these characters. The theoretically maximum conversion efficiency of QDSSCs (44%) (Hanna and Nozik, 2006) is considerably higher than that of DSSCs (31%).

The most efficient dye-sensitized solar cell was reported by O'Regan and Grätzel in 1991 where they reported exceptionally high efficiencies for the conversion of incident photons to electrical current of greater than 80%, giving an overall cell efficiency of 11% using a ruthenium based organic dye (O'Regan and Grätzel, 1991). This limits the cells light harvesting ability due to the dye complex containing a relatively low extinction

coefficient and having the possibility of electron recombination during the charge transfer process. Furthermore, organic dyes are intrinsically prone to photooxidation when exposed to heat and light, making it difficult to produce highly stable cells that are robust.

Another disadvantage of organic dyes is that only few of them can absorb a broad spectral range, making this an issue when trying to absorb the whole solar spectrum.

These disadvantages and the improved optical properties of QDs lead to QD sensitized photocatalysts to be superior. However, the inferior properties of QD-sensitized devices come along with difficulties in preparation. This problem was recognised by Zaban and Oron in 2011 who sought to widen the absorption spectra of dyes as well as improve the efficiency of the current dye-sensitized photovoltaic cells (Buhbut et al., 2010). The design incorporated both the use of organic dyes as well as QDs working simultaneously as sensitizers for a photovoltaic cell. The QD antennas transferred the energy of the absorbed light to the dye molecules resulting in a highly efficient energy transfer and improved performance of the device. Exchanging the use of organic dyes for QDs or using a combination of both therefore shows optimisation of light harvesting for use in photovoltaic devices (Macdonald and Nann, 2011).

2.7 Quantum Dots (QDs)

In recent years, the synthesis and characterization of quantum dots and nanoparticles of group II-VI compound semiconductors have generated a great deal of research interest because of their growing importance in technological applications, primarily due to the size and the shape dependence of their optical and electrical properties.

The semiconducting QDs exhibit size dependent spectral response when the dimensions of the particles are below the Bohr radius of that material. The smaller nanoparticles are observed to have considerably blue shifted absorption spectra due to quantum confinement effect. As the particle size approaches the Bohr radius of that material, the blue shift diminishes, and the particle properties resembles that of the bulk material. The property of size dependent bandgap of the QDs is highly desired for tuning the spectral response of the device to achieve selective absorption (Rasin, 2014).

As reported in Ahmed Tasnim Rasin's thesis, quantum dots (QDs) are semiconductor nanoparticles with theoretical 0-D structures, confined in three spatial dimensions. The material properties of QDs depend on the energy level of charges (electrons and holes). Confining the material spatially imposes limits on the motion or kinetic energy giving rise to quantization of the electron and hole energies. This leads to higher energy requirement to separate the charges in the semiconductor particles compared to that in the bulk. Decreasing particle size introduces such 3D confinement and variation of material properties such as optical bandgap, photoluminescence, extinction coefficient and energy transfer compared to their bulk behaviour is observed. Under this size constraint, the properties of quantum dots are a strong function of their particle size (Rasin, 2014).

The observation of multiple exciton generation (MEG) in colloidal QDs has triggered the interest in semiconductor QDs as light harvesting materials. Despite certain controversy, (Trinh *et al.*, 2008) very recently it has been demonstrated that internal quantum efficiencies higher than 100% in PbS nanocrystals are possible, if they are carefully coated on single

crystal TiO₂ substrates. (Sambur et al., 2010). The schematic diagram of working mechanism of the typical QDSSCs is shown in Figure 2.2.

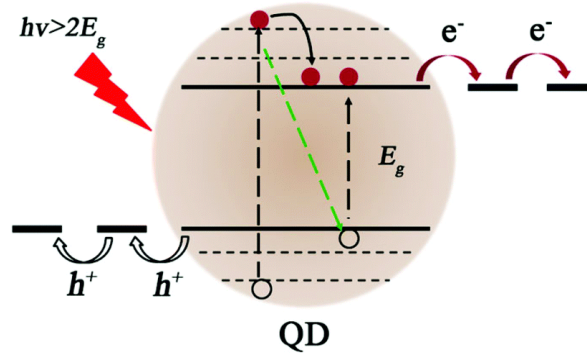


Figure 2.2: Schematic depiction of multiple exciton generation (MEG) and extraction (Zhang et al., 2015)

2.8 Quantum Confinement

Semiconductor particles start to show deviations in their optical properties when the particle dimensions are 2 – 3 times their Bohr radius (Ekimov *et al.*, 1993).

Every atom has electron revolving around its nucleus in a fixed path. Bohr radius represent the mean radius of electron around the nucleus of hydrogen atom in its lowest energy level. It is represented by the letter a . The concept of Bohr radius is based on the Bohr model of atom. According to this model, atom consists of small positively charged nucleus around which negatively charged electrons orbit in circular paths. But later researchers found that electron surround the nucleus in spherically shaped probability zone called shells. The radius of the Bohr orbit in atoms like hydrogen and species like hydrogen is given by the formula:

$$a = \frac{n^2 h^2}{4\pi^2 m e^2} \times \frac{1}{Z}$$

(Equation 2.1)

where m is the mass of electron,

e is the charge of electron,

h is the Planck's constant,

n is the principle quantum number of orbit, and

Z is the atomic number (Study)

When the electron confinement energy is smaller than the Coulomb attraction energy, the semiconductor behaviour shows weak confinement effects. If these energies are of the same order, intermediate confinement is observed. However, as the particle size (r) becomes smaller compared to Bohr radius ($r < a_0$), r^{-2} term dominates and the minimum energy to separate an electron-hole pair (E_{\min}) increases beyond its bulk value, for which strong confinement is observed (Rasin, 2014).

The reduction in the number of atoms in a material results in the confinement of normally delocalized energy states. Electron-hole pairs become spatially confined when the diameter of a particle approaches the de Broglie wavelength of electrons in the conduction band. As a result, the energy difference between the energy bands is increased with decreasing the particle size.

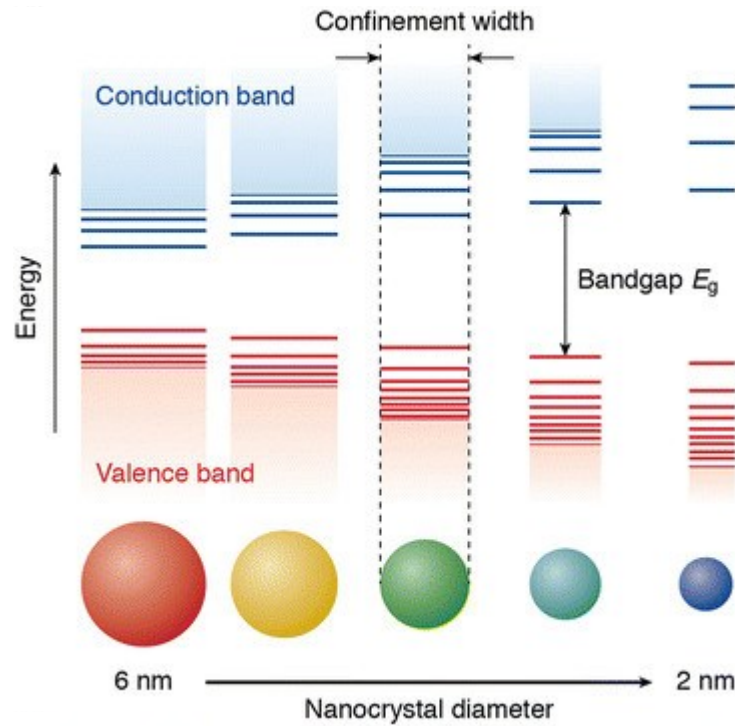


Figure 2.3: Quantum confinement in QDs (Rabouw and de Mello Donega, 2016)

2.9 ZnSe QDs

Regarding the inherent toxicity of these systems that may hinder a safe use in application, there is a natural seek for substituting cadmium ion sand producing less toxic materials. Aiming this biocompatibility some recent reports present doped and undoped ZnSe crystals in the quantum confinement region as potential materials in photovoltaic device (Nikesh *et al.*, 2006). Moreover, due to their intense UV blue luminescent properties—bulk $E_g = 2.7$ eV (460nm) which are not observed in other II–VI semiconductor materials, ZnSe crystals also show a great potential in application to low-voltage electroluminescent devices and blue diode lasers. Although the interest in ZnSe nanocrystalline materials has increased greatly in the last decade, there is not yet a synthetical procedure that can be used to produce well-defined nanocrystals in large amounts

which can be transposed to a large-scale production. ZnSe nanocrystals play an essential role in developing transition metal doped semiconductor nanocrystals (Pradhan *et al.*, 2005) as non-cadmium fluorescent nanocrystals.

2.10 Passivating Layer

It is well known that QDs have a large number of surface defect states, and surface passivation has a substantial influence on their chemical and optical properties including charge generation and separation processes. In the SILAR process, after QD growth typically a thin layer of ZnS is deposited to passivate the QD surface states, which can improve QD stability and promote electron injection from the QDs to the photoanode, and thus leads to enhanced QDSSC performance.

Earlier report shows that ZnS coating has successfully improved incident photon-to-current efficiency (IPCE) of CdS QDSSC, due to the expected surface defect modification and reduced recombination loss at the QD/electrolyte interface. However, further increasing ZnS coating cycles led to decreased device performance, which could be related to a suppressed regenerative process associated with thick ZnS coating layers. ZnS has wide band gap which is 3.91 eV, the conduction band edge is higher than that of CdS while its valance band edge is lower than that of CdS, it in fact created exciton confinement in the CdS QDs and thus prevented the occurrence of exciton delocalization (Qilin *et al.*, 2016).

2.11 Surface treatment

It has been shown that surface treatments were important in QDSSCs. They can be used to protect the semiconductor QDs or to allow the control of recombination processes and band alignment and electron injection in the solar cells.

2.11.1 Fluoride Treatment

As reported by Samadpour in 2011, there was an increase of solar performance after NH_4F treatment of a thin layer of TiO_2 for mesoporous metal oxide free CdSe solar cells. Decrease of reflectance is observed for PbS/CdS electrodes at long wavelengths. The shift of the absorption threshold to longer wavelengths has been previously observed as the number of PbS SILAR cycles increases, and it correlates to the growth of the PbS QDs. Consequently, a higher PbS loading is obtained after the fluorine treatment, despite the same number of SILAR cycles being performed for treated and untreated samples. This fact indicates a change in the reaction kinetics of the PbS deposition process by SILAR. The fluorine attached to the TiO_2 surface produces an acidification of the surface that probably enhances the dissociation of $\text{Pb}(\text{NO}_3)_2$, consequently increasing the deposition rate (Samadpour et al., 2011).

2.11.2 Chloride Treatment

TiCl₄ treatment on the transparent conductive oxide prior to TiO₂ nanoparticle deposition and also after sintering of the TiO₂ nanoparticles is conventionally carried out. The first TiCl₄ treatment aims at increasing the contact between TiO₂ nanoparticles and the conductive substrate, while the second treatment is responsible for a higher dye loading and a down-shift of the TiO₂ conduction band (CB) favoring the increase of photocurrent.

2.12 Advantages of QDs as Sensitizers

The advantages of the QD sensitizers over conventional dyes are their quantum-confinement effect (including impact ionization) and Auger recombination. These effects are known to increase the exciton concentration, quantum yield, hot-electron lifetime, and consequently the performance of QDSSCs. Another advantage of the QD sensitizers is their high extinction coefficient, which is known to reduce the dark current and increase the overall efficiency of a solar cell (Li et al., 2011).

2.13 Fabrication of QDs

There are two main processes of QD deposition: (a) solution-processed and (b) epitaxial process. SILAR and CBD methods belong to the first process. QDs made by these methods can be deposited directly on the substrate. These methods are discussed briefly in the following sections.

The QD particles can be fabricated directly on the TiO₂/FTO substrates using wet chemistry deposition methods such as successive ionic layer adsorption and reaction (SILAR) and chemical bath deposition (CBD) (Lee *et al.*, 2009)(Kamat, 2008).

2.13.1 Successive Ionic Layer Adsorption and Reaction (SILAR)

This method is suitable for fabricating binary semiconductor compounds like CdS, CdSe, ZnS, PbS, etc. This is an in-situ deposition method where QDs are adsorbed on the substrate by immersing it alternatively in cationic and anionic precursor solutions (Figure 2.4). The cations are adsorbed on the substrate by dipping the substrate inside the cationic solution first. The substrate is subsequently rinsed with a solvent and dried in argon or nitrogen gas flow.

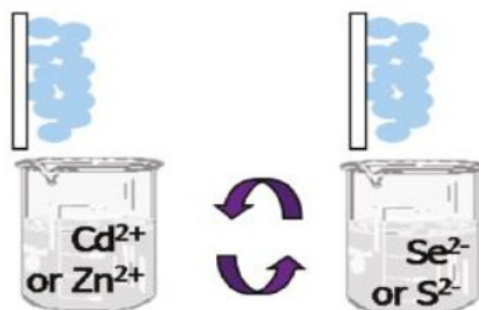


Figure 2.4: Schematic representation of SILAR deposition (Lee *et al.*, 2010)

Rinsing is required to wash off excess ions from the substrate which allows for better control of particle size. The electrodes are then dipped in the anionic precursor solution and later rinsed and dried. The anions attach to the adsorbed cation layer and form nanoparticles

through nucleation process. This completes one cycle. Repeating the number of cycles lets the particles grow in a controlled manner. Other factors that can influence the growth mechanism, such as dipping time, precursor concentration and reaction temperature are kept constant allowing the particle growth to be controlled solely by the number of deposition cycles.

Earlier reports by Kale and Lokhande, reveal that SILAR deposited ZnSe thin films synthesized using acidic cationic precursor solution are of poor crystallinity, although long duration annealing resulted in the evolution of diffraction peaks indicating the polycrystalline nature of the films (Kale and Lokhande, 2004). In the present investigation ZnSe thin films are synthesized at room temperature employing SILAR technique using an alkaline cationic precursor solution.

As reported by Qilin, QDs prepared with one SILAR cycle produced the lowest IPCE efficiency, which was associated with the limited light harvesting capability due to a low QD coverage. As the number of SILAR coating cycles was increased, IPCE also increased due to improved QD coverage. The IPCE of the device prepared with five coating cycles showed the best efficiency, and further increasing the SILAR cycles led to decreased IPCE. This phenomenon could be attributed to the increased recombination losses caused by a multilayer QD structure that was related to excessive SILAR coating cycles. In addition, when the SILAR coating cycles were high, such as the six- and seven-cycle depositions, the thick intermediate QD layer could also substantially block electron and hole collections because these carriers did not have direct contact with the photoanode and the electrolyte, respectively, which could cause decreased charge collection efficiency and further lower the

IPCE performance. For the QDs that are synthesized using the SILAR method, each additional SILAR coating cycle not only increases the QD density and coverage, but can also simultaneously increase the QD size due to more material deposition on the surface of the QDs that are synthesized in the previous cycles (Qilin et al., 2016).

2.13.2 Chemical Bath Deposition (CBD)

This is an in-situ method for QD deposition but instead of two precursor solutions used in the SILAR approach, only one precursor solution is needed for material deposition by CBD method (Rühle, Shalom and Zaban, 2010). The precursor solution in this case contains both the cations and anions to be deposited on the substrate. The solution pH and temperature for CBD needs to be controlled with care. The need for more precursor materials and longer deposition times makes CBD less attractive for QD fabrication as compared to SILAR. This method is used for fabricating thin semiconductor layers as well as QDs.

In reports of Shah, with CBD method, effect of concentration of Na_2SeSO_3 on the absorption spectra of the synthesized CdSe nanoparticles was studied by fixing concentration of $\text{Cd}(\text{OAc})_2$. The excitonic absorption shows a red shift, on decreasing the $[\text{Cd}(\text{OAc})_2]/[\text{Na}_2\text{SeSO}_3]$ ratio, which indicates an increase in the size of the nanoparticles. The probable reason for the formation of CdSe nanoparticles of larger size at lower concentration of $\text{Cd}(\text{OAc})_2$, or vice versa, could be due to the mechanism of nanoparticle formation. Cd^{2+} ions are freely available from the $\text{Cd}(\text{OAc})_2$ precursor, whereas the counter part is released from SeSO_3^{2-} much slower. Therefore, the concentration of $\text{Cd}(\text{OAc})_2$ governs the number of nucleation sites available for the growth of CdSe

nanoparticles. For a given concentration of selenium precursor, the greater the number of nucleation sites, the smaller will be the size of the CdSe nanoparticles formed. Similarly, for a given concentration of Cd(OAc)₂, the number of nucleation sites remains more or less same, and with an increase in the concentration of Na₂SeSO₃, the particles size is expected to increase (Shah et al., 2010).

2.14 Applications

Quantum dot-sensitized solar cells (QDSSCs) are considered as a promising candidate for the development of next generation solar cells because they can be fabricated by simple and low-cost techniques (O'Regan and Grätzel, 1991). The development of nanotechnology, especially the synthesis and application of nanomaterials, facilitates the progress of QDSSCs and enables them to receive more and more interests. Currently, the efforts on improving the performance of QDSSCs have mainly been focused on fundamental issues, such as improved understanding of device physics, optimization of device structure by advanced processing methods and development of high-performance materials (Yang et al., 2002). These combined efforts have led to very encouraging power conversion efficiency of 4.22% (Lee and Lo, 2009). However, such efficiency is far away for the practical applications. As a result, further exploration on the optimization of QDSSC performance is necessary.